ACS OMEGA

http://pubs.acs.org/journal/acsodf

Article

Demonstrating the Potential of Alkali Metal-Doped Cyclic $C_6O_6Li_6$ Organometallics as Electrides and High-Performance NLO Materials

Sunaina Wajid,[⊥] Naveen Kosar,[⊥] Faizan Ullah, Mazhar Amjad Gilani, Khurshid Ayub, Shabbir Muhammad, and Tariq Mahmood*

Cite This: *ACS Omega* 2021, 6, 29852−29861

Read Online

ACCESS | Metrics & More | Article Recommendations

ABSTRACT: In this report, the geometric and electronic properties and static and dynamic hyperpolarizabilities of alkali metal-doped $C_6O_6Li_6$ organometallics are analyzed via density functional theory methods. The thermal stability of the considered complexes is examined through interaction energy (E_{int}) calculations. Doping of alkali metal derives diffuse excess electrons, which generate the electride characteristics in the respective systems (electrons@complexant, e^-@M@$C_6O_6Li_6$, M = Li, Na, and K). The electronic density shifting is also supported by natural bond orbital charge analysis. These electrides are further investigated for their nonlinear optical (NLO) responses through static and dynamic hyperpolarizability analyses. The potassium-doped $C_6O_6Li_6$ (K@$C_6O_6Li_6$) complex has high values of second- ($\beta_{tot} = 2.9 \times 10^5$ au) and third-order NLO responses ($\gamma_{tot} = 1.6 \times 10^8$ au) along with a high refractive index at 1064 nm, indicating that the NLO response of the corresponding complex increases at a higher wavelength. UV−vis absorption analysis is used to confirm the electronic excitations, which occur from the metal toward $C_6O_6Li_6$. We assume that these newly designed organometallic electrides can be used in optical and optoelectronic fields for achieving better second-harmonic-generation-based NLO materials.

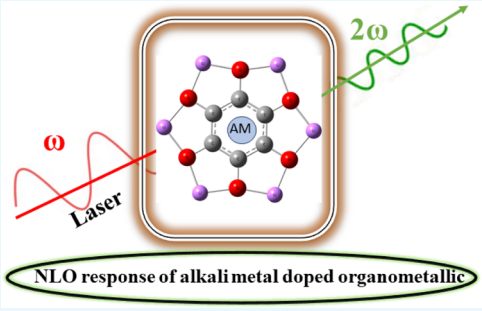

1. INTRODUCTION

Interest in designing high-performance nonlinear optical (NLO) materials is growing rapidly due to their widespread applications in optical computing,[1−3] optical communication,[4,5] optical switching,[6,7] optical logic functions,[8,9] dynamic image processing,[10,11] and many other optoelectronic fields.[12−17] Recently, a unique class of compounds known as electrides having isolated excess electrons has garnered great interest from the chemical society.[18−21] Due to this nontrivial electronic structure, they are easily polarizable and can serve as superior nonlinear optical materials.[19,22,23] Electrides due to their certain interesting properties such as the ultralow work function, relatively high catalytic activity, high electronic mobility, and optical and anisotropic properties have great potential for various applications.[24−28] In 1983, Dye and co-workers fabricated the first organic crystalline electride consisting of organic complexant cages in which alkali metals and electrons were trapped.[29] Since then, various organic and inorganic electrides have been reported in literature, and their novel electronic structures have been investigated both computationally and experimentally.[30−33]

Johnson and co-workers performed density functional theory (DFT) investigation for describing the organic electronic structure of eight organic electrides and confirmed the presence of localized interstitial electrons and hence defined their electride properties.[34] Kim et al. studied organic magnetic electrides in which they used maximally localized Wannier functions to identify the "cavity" electrons and the "empty atom" technique.[35] Saha et al. prepared synthetically viable neutral $[Mg_4(^{Dipp}{}_HL)2]^{2-}\cdot 2[K@CE]^+$ (CE = 18-crown-6 ether), containing four magnesium atoms and two Mg−Mg bonds, where the latter one act as an electride.[36] Dale and Johnson also used the DFT method for reproducing the known antiferromagnetic behavior of organic electrides.[24,37] Organic electrides are thermally less stable, so research is shifted toward the design and synthesis of thermally stable inorganic electrides.[24,38,39] Hosono and co-workers synthesized the first room-temperature-stable inorganic electride $Ca_6Al_7O_{16}$ ($C_{12}A_7$:$2e^-$) via oxygen-reduction processes while starting from the mineral mayenite ($12CaO\cdot 7Al_2O_3$).[40] Since then, $C_{12}A_7$:$2e^-$ has been used for ammonia synthesis[41] and as an electron-injection barrier material.[42] The discovery of $C_{12}A_7$:$2e^-$ has stimulated many new efforts to search for other inorganic electrides. Zhang et al. designed 33 hitherto unexpected structure prototypes of inorganic electrides

Received: August 12, 2021
Accepted: October 19, 2021
Published: October 29, 2021

through computer-assisted methods, in which 19 are not in the known structure databases.[43] Boldyrev and co-workers studied electride-like features in the MgO crystal with the defect F-centers. Their calculations show that the corresponding electride-like cluster possesses a noticeably large first hyperpolarizability (β_o = 5733 au).[44] Wang et al. designed bipyramidal CaN_3Ca by using quantum mechanical methods. They observed that these inorganic aromatic Robin−Day-type superalkali electrides have high sensitivity for use in multistate nonlinear optical switches.[45] The design and synthesis of organic and inorganic electrides continues because of their applications in catalysis, metal-ion batteries, NLO materials, and so forth Recently, transition-metal-based organometallics have been reported to exhibit a better second-harmonic generation (SHG) response.[46−49]

From the literature, it has been revealed that introducing excess electrons into a molecule can remarkably enhance the first hyperpolarizability (β_o).[50,51] The first hyperpolarizability (β_o) is the key factor which determines the presence of the NLO response in materials.[52,53] Many studies have been conducted to investigate the first hyperpolarizability (β_o) of different materials.[54−56] Computational work on the electride-type structure of Mg_4O_3 showed that Mg_4O_3 has pronounced NLO properties because it exhibited a large value of hyperpolarizability, that is, β_o = 5733.46 au.[44] Meanwhile, the strategy of metal adsorption on isolated surfaces has been introduced in recent years to further enhance the NLO properties. In this regard, many computational chemists studied the effect of alkali metal doping on NLO responses. As we know, alkali metals have a low ionization energy, due to which they can easily donate electrons to the system and results in an increase of the electron number. Thus, the NLO response will be enhanced due to the increasing number of electrons.[57−59] For example, the doping of inorganic $Al_{12}N_{12}$ nanocages into alkali metals narrowed the highest occupied molecular orbital (HOMO)−lowest unoccupied molecular orbital (LUMO) gap to a range of 0.49−0.71 eV. Furthermore, the value of hyperpolarizability (β_o) is also increased, which resulted in a large NLO response.[60,61]

Various alkali metal-doped organic electrides have been reported in literature with a large NLO response. For example, the alkali-metal-doped organic complexes (Li@calix4pyrrole and Li^+(calix4pyrrole)M^-) have been reported by Yu and co-workers as effective NLO materials because of their high values of hyperpolarizability (ranging from 10,969 to 35,934 au).[62] Similarly, alkali metal-doped organic fluorocarbon chains of $H-(CF_2-CH_2)_3-H$ with a high NLO response have been studied. Six different structures of Li atom-doped fluorocarbon complexes [Li_n-$H-(CF_2-CH_2)_3-H$ (n= 1, 2] have been examined. Among them, the highest NLO response of 76,978 au was recorded.[63] Recently, another electride $Li^+(C_{20}H_{15}Li_5)$-e^- modified by lithiation of the dodecahedron has been investigated computationally. In this electride, the C_{20} closed cage not only acts as a barrier for lithium ions but also has a negative inner electric field to stabilize the Li ion. Here, the excess electrons are released, which remain encapsulated in the Li_5 cavity. Thus, $Li^+(C_{20}H_{15}Li_5)e^-$ exhibits a large value of hyperpolarizability (1.4×10^4 au) with potential for application in NLO materials.[64] Mahmood and co-workers analyzed the organometallic C_6O_6 surface for the NLO response. They doped superalkalis on the C_6O_6 surface and achieved electride characteristics in their designed complexes with large hyperpolarizability.[65] $C_6O_6Li_6$ is obtained from lithium-ion batteries, as a result of redox reactions of electrodes. Cyclohexane is the precursor of this compound in lithium-ion batteries. Pure $C_6O_6Li_6$ and alkali metal-doped $C_6O_6Li_6$ are used here to study their NLO properties. We expect that the doped organometallics might show high values of induced dipole moment, polarizability, hyperpolarizability, and a high NLO response. The reason might be the increase in electronic density diffusion from the dopant to the surface or vice versa. Among alkali metals, lithium, sodium, and potassium are taken into account for doping on the $C_6O_6Li_6$ organometallic surface, and their electronic and NLO properties are comparatively studied.

2. RESULTS AND DISCUSSION

2.1. Geometries, Thermodynamic Stabilities, and Electride Characteristics of Alkali Metal (Li, Na, and K)-Doped $C_6O_6Li_6$ Organometallics. The energy minimum structure of $C_6O_6Li_6$ is shown in Figure 1, which is optimized at the ωb97XD/6-31+G(d,p) level of theory. It has a planar and star-like geometry having C−C, C−O, and O−Li bond lengths of 1.42, 1.38, and 1.79 Å, respectively. The alkali metal (Li, Na, and K)-doped M@$C_6O_6Li_6$ complexes are also

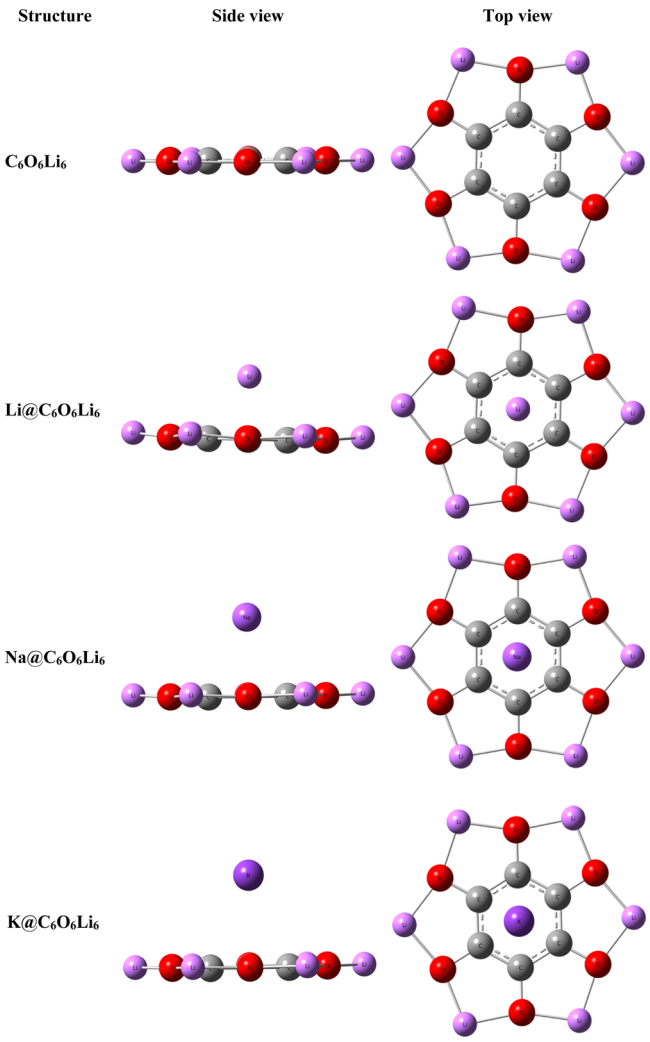

Figure 1. Side and top views of the optimized geometry of pristine $C_6O_6Li_6$ and alkali metal (Li, Na, and K)-doped $C_6O_6Li_6$ organometallics calculated at the ωB97XD/6-31+G(d,p) level.

https://doi.org/10.1021/acsomega.1c04349
ACS Omega 2021, 6, 29852−29861

Table 1. Smallest M-Ring Distance ($d_{M\text{-}ring}$, M = Li, Na, and K); NBO Charges on Carbon (Q_c), NBO Charges on Oxygen (Q_o), and NBO Charges on Lithium (Q_{Li}) of the $C_6O_6Li_6$ Nanocluster; NBO Charges on the Metal Dopant (Q_M, M = Li, Na, and K); Interaction Energies (E_{int}); and Vertical Ionization Energies (IE_v)

systems	$d_{M\text{-}ring}$ (Å)	Q_C (lel)	Q_o (lel)	Q_{Li} (lel)	Q_M (lel)	E_{int} kcal mol^{-1}	IE_v eV
$C_6O_6Li_6$		0.176	−1.122	0.947			4.39
$C_6O_6Li_6$−Li	1.95	0.133	−1.089	0.951	0.033	−27.11	2.82
$C_6O_6Li_6$−Na	2.46	0.147	−1.099	0.952	0.007	−19.30	3.03
$C_6O_6Li_6$−K	2.80	0.154	−1.106	0.951	0.015	−19.46	2.73

optimized at the same level of theory as shown in Figure 1. After optimizing the metal-doped organometallics, the bond lengths observed are 1.41, 1.37, and 1.81 Å for C−C, C−O, and C−Li, respectively. These minute changes in bond lengths confirm that structural integrity of the organometallic complex remains preserved after doping. The interaction distance of the Li metal from the center of ring is 1.95 Å, whereas for Na and K these are 2.46 and 2.80 Å, respectively. A monotonic trend of an increasing interaction distance, with an increase in the atomic number, from the center of the ring is observed, and this is similar to the already reported results.[66] The interaction energy of the system reveals that the thermodynamic stability of any system that is highly exothermic in nature reflects a greater thermodynamic stability.[67] The interaction energies of these alkali metal-doped M@$C_6O_6Li_6$ complexes are given in Table 1. The $E_{int.}$ values of Li@$C_6O_6Li_6$, Na@ $C_6O_6Li_6$, and K@$C_6O_6Li_6$ organometallics are −27.11, −19.30, and −19.46 kcal mol^{-1}, respectively. Among the three considered organometallics, the most stable one is the Li@$C_6O_6Li_6$ complex due to the least interaction distance of Li with the complexant (vide supra) and hence a stronger interaction. The reason for the high thermal stability of Li-doped complexes is the low ionization potential and a smaller atomic size of the Li metal and thus is considered as the best adsorbing species on the C_{20} nanocage. The results are comparable to those of the work reported by Mahmood and co-workers on single and multiple alkali-doped C_{24} nanocages.[66]

To investigate the electride characteristics and electronic properties of M@$C_6O_6Li_6$ organometallic complexes, Frontier molecular orbital analysis is performed. The energies of HOMOs, LUMOs, and the corresponding HOMO−LUMO (H−L_{gap}) energy gaps of pure $C_6O_6Li_6$ and alkali metal-doped organometallics are presented in Table 2. The calculated energy gap (H−L_{gap}) of pure $C_6O_6Li_6$ is 4.64 eV. The decoration of alkali metals on the surface resulted in a decrease of the corresponding H−L_{gap} (2.77−3.12 eV). The energies of the HOMO, LUMO, and the corresponding H−L_{gap} of the Li@$C_6O_6Li_6$ complex are −2.73, 0.08, and 2.9 eV, respectively. For Na@$C_6O_6Li_6$, the energies of the HOMO, LUMO, and H−L_{gap} are −3.03, 0.09, and 3.12 eV, respectively. Similarly, in the case of the K@$C_6O_6Li_6$ complex, they are −2.73, 0.04, and 2.77 eV, respectively. The decreased H−L gaps reflect the conducting behavior of all newly designed organometallics.[66] The decrease in H−L_{gap} is due to the formation of new HOMOs at high energy because of the presence of excess electrons. These excess electrons are introduced by electropositive alkali metals.[68,69]

From the pictorial representation of isodensities of HOMOs of pure $C_6O_6Li_6$ and alkali metal-doped organometallics (Figure 2), it is observed that the electronic density of HOMOs of the Li@$C_6O_6Li_6$ and Na@$C_6O_6Li_6$ organometallics mainly resides in empty space (does not shared by any atom), which proves their electride characteristics.[65,70,71]

Table 2. Dipole Moment (in Debye), Polarizability (α_o), Static First Hyperpolarizability (β_o), Vector-Based Static First Hyperpolarizability (β_{Vec}), Static Second Hyperpolarizability (γ_{tot}), Oscillator Strength (f_o), Transition Energy (ΔE), the Variational Dipole Moment Z Component between the Ground and Crucial Excited States ($\Delta\mu$), β_Z under the Two-Level Model, the Energies of HOMO (E_{HOMO}), the Energies LUMO (E_{LUMO}), and the HOMO−LUMO Gaps (H−L_{gap} in eV)[a]

parameters	$C_6O_6Li_6$	$C_6O_6Li_6$−Li	$C_6O_6Li_6$−Na	$C_6O_6Li_6$−K
μ_o (au)	0.01	5.96	6.34	7.84
α_o (au)	136	608	503	558
$*^1\beta_o$ (au)	2.3×10^2	8.7×10^4	1.4×10^5	2.9×10^5
$*^2\beta_o$ (au)	1.9×10^2	4.7×10^4	4.9×10^4	2.5×10^5
β_{vec} (au)	4.13	8.4×10^4	8.3×10^3	2.7×10^5
β_{HRS} (au)	1.60	3.8×10^4	2.9×10^5	8.4×10^3
γ_{tot} (au)	2.3×10^5	9.7×10^7	3.4×10^7	1.6×10^8
f_o		0.20	0.22	0.11
sΔE (eV)	2.39	1.45	1.59	1.02
$\Delta\mu$ (Debye)		0.01	0.11	5.35
β_Z (au)		1.1×10^3	4.3×10^3	1.2×10^5
E_{HOMO} (eV)	−4.39	−2.82	−3.03	−2.73
E_{LUMO} (eV)	0.24	0.07	0.09	0.04
H−L_{gap} (eV)	4.63	2.89	3.12	2.77

[a] $*^1\beta_o$ (au) and $*^2\beta_o$ (au) represent hyperpolarizability at the ωB97XD and LC-BLYP levels, respectively.

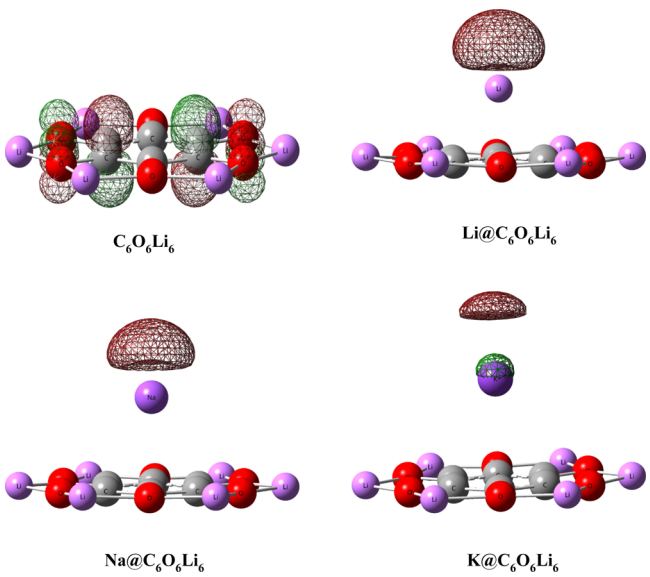

Figure 2. Graphical representation of HOMO of pristine $C_6O_6Li_6$ and alkali metal-doped $C_6O_6Li_6$ organometallics (isovalue = 0.05).

The electride features of these both organometallics (Li@ $C_6O_6Li_6$ and Na@$C_6O_6Li_6$) originate due to the presence of an

https://doi.org/10.1021/acsomega.1c04349
ACS Omega 2021, 6, 29852−29861

intramolecular push−pull mechanism. The isolated $C_6O_6Li_6$ molecule first pulls the valence s-shell electrons of the alkali metal to form an anion and then the resulting anion pushes these electrons to produce isolated excess electrons. In these newly designed electrides, the electronic density is present mainly near the alkali metal, which reflects the more contribution of alkali metal as compared to $C_6O_6Li_6$. An exceptional behavior is observed for the K@$C_6O_6Li_6$ complex, wherein the electronic density mainly resides over K, reflecting the simple excess electron system instead of the electride character.[50,65]

As the electrides contain a loosely bound electronic density, not belonging to any atom, the electronic stability is very important, which is directly related to the vertical ionization energies.[43,72] Both electrides, Li@$C_6O_6Li_6$ and Na@$C_6O_6Li_6$, possess sufficiently high vertical ionization energies of 2.83 and 3.03 eV, respectively, which is indicative of their electronic stability.

Natural bond orbital (NBO) charge analysis revealed that the alkali metal is positively charged, whereas the negative charge on the complexant is increased. This indicates that charge is transferred from the metal to the $C_6O_6Li_6$ ring. The average NBO charge on the Li atom (0.033 |e|) is comparatively higher than those of Na (0.007 |e|) and K (0.015 |e|) atoms. The reason for a higher charge on Li represents the ease in releasing electrons due to its smaller size and low ionization energy as observed by Biglari and co-workers.[73] In all these organometallics, alkali metals donate the electronic density to the $C_6O_6Li_6$ surface due to their low ionization energies compared to other metal atoms and are considered as the source of excess electrons for the generation of electride properties in the respective complexes.

2.2. Static and Dynamic Hyperpolarizability Analyses of Newly Designed Electrides for NLO Applications. *2.2.1. Static Hyperpolarizability Analysis.* All parameters, which are responsible for the effective NLO response of the newly designed organometallics (electrides), are given in Table 2. The dipole moment of isolated $C_6O_6Li_6$ is 0.0 D due to its symmetry. However, the doping of alkali metals results in charge transfer, thus breaking the symmetry, which in turn increases the dipole moment. The dipole moments of Li@$C_6O_6Li_6$, Na@$C_6O_6Li_6$, and K@$C_6O_6Li_6$ organometallic complexes are 5.96 D, 6.34 D, and 7.84 D, respectively. The monotonic trend of the increase in the dipole moment reflects the more charge separation of charges with an internuclear distance, going from Li to K, which is indicative of their possible linear and nonlinear optical potential, similar to the work of Cherepanov and co-workers.[74] For investigation of the linear optical response, the mean static polarizabilities (α_o) of newly designed electrides and the excess electron complex are investigated as well. α_o of M@$C_6O_6Li_6$ complexes is in the range of 503 to 608 au, which is very high as compared to that of the pure $C_6O_6Li_6$ (136 au). The nonmonotonic trend of the increase in α_o is observed as follows; Li@$C_6O_6Li_6$ > K@$C_6O_6Li_6$ > Na@$C_6O_6Li_6$. The trend of polarization is governed by the charge transfer. More charge is transferred in the case of Li (0.033 |e|), followed by K (0.015 |e|), while less charge is shifted from the Na metal (0.007 |e|). Subsequently, this charge separation causes polarization changes in these organometallics.

Furthermore, the NLO response of alkali metal-doped M@$C_6O_6Li_6$ (M = Li, Na, and K) complexes (electrides) is confirmed by computing their static first hyperpolarizabilities (β_o) at the LC-BLYP and ωB97XD levels with a similar 6-311++G (2d,2p) basis set (Table 2). The β_o value of the pristine system is relatively small (1.9×10^2 au at LC-BLYP and 2.3×10^2 au at ωB97XD). The β_o values of the M@$C_6O_6Li_6$ (M = Li, Na, and K) complexes (electrides) range from 4.7×10^4 to 2.5×10^5 au at the LC-BLYP level. At the ωB97XD level, the β_o values of the M@$C_6O_6Li_6$ (M = Li, Na, and K) complexes (electrides) range from 8.7×10^4 au to 2.9×10^5 au. Despite the small differences in their values with different functionals, the trend of hyperpolarizabilities is quite comparable. The similar values and the same trend of hyperpolarizability with both functionals are due to the same 1.00 fraction of nonlocal exchange. As a result of doping of alkali metals, a remarkable NLO response of M@$C_6O_6Li_6$ electrides is observed and the static first hyperpolarizability (β_o) is tremendously increased. β_o values of the newly designed electrides and the excess electron system are in the range of 3.4×10^4 to 2.9×10^5 au. The highest β_o is observed for K@$C_6O_6Li_6$, that is, of 2.9×10^5 au, while the lowest value is computed for the Li@$C_6O_6Li_6$ electride. The results revealed the monotonic increasing trend of β_o, and it increases from Li@$C_6O_6Li_6$ to K@$C_6O_6Li_6$. This monotonic behavior of the designed electrides can be correlated with the vertical ionization potential, which is the major factor that affects the β_o value. It increases with the decrease in vertical ionization energy.[75−77] The K@$C_6O_6Li_6$ complex has the lowest vertical ionization energy (−2.73 eV) among all organometallics (Na@$C_6O_6Li_6$ = −2.73 eV and Li@$C_6O_6Li_6$ = −2.73 eV), and exhibits the largest nonlinear optical response (2.9×10^5 au). To gain further insights into factors affecting the β_o values of the designed electrides, we calculated the β_z values by employing a two-level model using Multiwfn software.[78] The β_z values from the two-level model nicely correlate with our computed values of first hyperpolarizability (β_o). From the two-level model, it can be observed that the crucial excitation energy is the dominant factor in determining the first hyperpolarizability values of the electrides. The crucial excitation energies of Li@$C_6O_6Li_6$, Na@$C_6O_6Li_6$, and K@$C_6O_6Li_6$ are 1.45, 1.59, and 1.02 eV, respectively. Because (β_o) is inversely proportional to the cube of crucial excitation energy, the β_o value of K@$C_6O_6Li_6$ is large, but the crucial excitation energy is low; on the other hand, the β_o value of Li@$C_6O_6Li_6$ is small, while the crucial excitation energy is large. An exceptional behavior is observed for Na@$C_6O_6Li_6$, where the excitation energy is large (1.59 eV); however, β_o for this complex is also high (1.4×10^5 au). Besides the excitation energy, β_{tot} is directly proportional to $\Delta\mu$. The trend in the values of $\Delta\mu$ is the same as that in the values of first static hyperpolarizability. It can be concluded that $\Delta\mu$ is a major factor, which influences the hyperpolarizability of the complexes (as shown in Table 2). The trend of increasing β_o and $\Delta\mu$ is Li@$C_6O_6Li_6$ ($\beta_o = 8.7 \times 10^4$ au and $\Delta\mu$ = 0.01 eV) < Na@$C_6O_6Li_6$ ($\beta_o = 1.4 \times 10^5$ au and $\Delta\mu$ = 0.11 eV) < K@$C_6O_6Li_6$ ($\beta_o = 2.9 \times 10^5$ au and $\Delta\mu$ = 5.35 eV).

β_{vec} values of alkali metal-doped M@$C_6O_6Li_6$ (M = Li, Na, and K) electrides are calculated and provided in Table 2. β_{vec} is the projection of the first hyperpolarizability along the dipole moment vector and is a more reliable factor for predicting the NLO properties.[79] Among all M@$C_6O_6Li_6$ electrides, the dipole moment vector lies on the z-axis. The β_{vec} values of Li@$C_6O_6Li_6$, Na@$C_6O_6Li_6$, and K@$C_6O_6Li_6$ are 8.4×10^4, 8.3×10^3, and 2.7×10^5 au, respectively. It is observed that β_{vec} values are very much comparable with the first hyperpolarizability (β_o) results. The trend of increasing β_{vec} value

https://doi.org/10.1021/acsomega.1c04349
ACS Omega 2021, 6, 29852−29861

Table 3. Frequency-Dependent First Hyperpolarizability (β in au), Second Hyperpolarizability (γ in au), and the Nonlinear Refractive Index (n_2 in cm^2 W^{-1}) of Designed Electrides (Complexes) M@$C_6O_6Li_6$ (M = Li, Na, and K)

parameters	frequency ω	$C_6O_6Li_6$	C6O6Li6−Li	C6O6Li6−Na	C6O6Li6−K
$\beta(-\omega,\omega,0)$ (au)	0.000	4.1×10^0	8.4×10^4	8.9×10^3	2.7×10^5
	0.0428 (1064 nm)	6.7×10^0	5.9×10^5	4.3×10^5	4.3×10^5
	0.856 (532 nm)	1.0×10^3	3.5×10^5	7.3×10^5	2.6×10^4
$\beta(-2\omega,\omega,\omega)$ (au)	0.000	4.1×10^0	8.4×10^4	8.9×10^3	2.7×10^5
	0.0428 (1064 nm)	7.4×10^1	3.0×10^5	3.8×10^5	2.7×10^5
	0.0856 (532 nm)	3.5×10^3	9.3×10^4	6.5×10^5	1.7×10^4
$\gamma(-\omega;\omega,0,0)$ (au)	0.000	2.3×10^5	9.8×10^7	3.3×10^7	1.6×10^8
	0.0428 (1064 nm)	3.7×10^5	2.0×10^8	1.4×10^9	1.4×10^8
	0.0856 (532 nm)	5.2×10^8	1.5×10^{11}	1.3×10^9	3.5×10^6
$\gamma(-2\omega;\omega,0,0)$ (au)	0.000	2.3×10^5	9.8×10^7	3.3×10^7	1.6×10^8
	0.0428 (1064 nm)	1.5×10^7	1.5×10^9	3.8×10^8	4.7×10^7
	0.0856 (532 nm)	5.0×10^7	5.9×10^{10}	1.2×10^9	5.4×10^6
γ^{DFWM} $(-\omega;\omega,-\omega,\omega)$ (au)	0.0428 (1064 nm)	3.4×10^7	3.6×10^9	1.5×10^{10}	2.4×10^7
	0.0856 (532 nm)	6.1×10^{10}	2.7×10^{13}	6.4×10^{10}	4.85×10^4
n_2 (cm^2 W^{-1})	0.0428 (1064 nm)	2.8×10^{-15}	3.0×10^{-13}	12.9×10^{-13}	2.0×10^{-16}
	0.0856 (532 nm)	5.1×10^{-12}	2.2×10^{-12}	5.3×10^{-13}	4.0×10^{-19}

(2.7×10^5 au) for K@$C_6O_6Li_6$ is almost similar to that of β_o (2.9×10^5 au).

Hyper-Rayleigh scattering (HRS) is a very useful experimental technique for the direct measurement of the static hyperpolarizability values.[75,80] β_{HRS} values along with the depolarization ratio (DR) of all newly designed electrides and the diffuse excess electron system are calculated, and the values are given in Table 2. The observed trend of β_{HRS} values is as follows; Na@$C_6O_6Li_6$ (2.9×10^5 au) > Li@$C_6O_6Li_6$ (3.8×10^4 au) > K@$C_6O_6Li_6$ (8.4×10^3 au). The DR values of pure and alkali metal-doped organometallics, that is, Li@$C_6O_6Li_6$, Na@$C_6O_6Li_6$, and K@$C_6O_6Li_6$, are 1.5, 3.1, and 3.4, respectively. β_{HRS} depends on the polarization angle, and it is observed that pristine $C_6O_6Li_6$ and the corresponding alkali metal-doped organometallics (Na@$C_6O_6Li_6$ and K@$C_6O_6Li_6$) are octupolar molecules with an octupolar contribution of Φ (βJ = 3) of 89.6, 58.8, and 56.6%, respectively.

2.2.2. Frequency-Dependent (Dynamic) Hyperpolarizability Analysis. For explaining the high accuracy of the results and gaining insights for the experimental utility, we computed the frequency-dependent first hyperpolarizability coefficients that include electro-optic Pockel's effect (EOPE) with $\beta(-\omega;\omega,0)$ and SHG of first hyperpolarizability with $\beta(-2\omega;\omega,\omega)$ at the routinely used laser wavelengths of 532 and 1064 nm, respectively. The detailed values are given in Table 3. The dynamic first hyperpolarizability parameters are always dependent on wavelengths. At 532 nm, the values of EOPE range from 2.6×10^4 to 7.3×10^5, and at 1064 nm of wavelength these are from 4.3×10^5 to 5.8×10^5 au. Both electrides, Li@$C_6O_6Li_6$ and Na@$C_6O_6Li_6$, have their maximum EOPE values at 532 and 1064 nm, respectively, indicating the resonant enhancement of these at respective wavelengths, while for K@$C_6O_6Li_6$ the resonant enhancement occurs at 1064 nm (4.3×10^5 au). Similarly, $\beta(-2\omega;\omega,\omega)$ values reflecting the SHG response range from 1.7×10^4 to 6.5×10^5 au at a wavelength of 532 nm and range from 2.7×10^5 to 3.8×10^5 au at a wavelength of 1064 nm. At 532 nm, the highest SHG value has been computed for the Na@$C_6O_6Li_6$ complex, while both Li@$C_6O_6Li_6$ and K@$C_6O_6Li_6$ organometallics have shown the strong SHG response at 1064 nm.

2.2.3. Third-Order Nonlinear Optical Response. The third-order nonlinear optical response of the respective complexes was determined, and the dc-Kerr effect $\gamma(-\omega;\omega,0,0)$, the electric field-induced SHG(ESHG), and the quadratic nonlinear refractive index of organometallics at 532 and 1064 nm were computed. The results emphasize that $C_6O_6Li_6$ and Li@$C_6O_6Li_6$ have the highest responses for the dc-Kerr effect $\gamma(-\omega;\omega,0,0)$ at 532 nm; on the other hand, Na@$C_6O_6Li_6$ and K@$C_6O_6Li_6$ have their highest values at 1064 nm. It is reflected from the results that all organometallics except the K-doped complex have their highest values of the ESHG response at 532 nm. The remarkably high ESHG and the dc-Kerr effect $\gamma(-\omega;\omega,0,0)$ values of $C_6O_6Li_6$−K at high wavelengths indicate that the response of this organometallic complex can be enhanced by increasing the wavelength of incident light.

The four degenerate wave mixing values are calculated by using the second hyperpolarizability coefficients, then the nonlinear quadratic refractive index is calculated from γ^{DWFM} by using the equation shown below

$$n_2(\text{cm}^2\,\text{W}^{-1}) = 8.28 \times 10^{-23}\gamma^{DFWM}\ (\text{au}) \quad (1)$$

The results of n_2 are shown in Table 3. The quadratic nonlinear refractive index values of all doped organometallics are high at 532 nm, that is, 2.2×10^{-12} au (Li@$C_6O_6Li_6$) and 5.3×10^{-13} au (Na@$C_6O_6Li_6$), except for the potassium doped complex (K@$C_6O_6Li_6$ = 2.0×10^{-16} au), which has a high value of quadratic nonlinear refractive index at 1064 nm. Among all these organometallics, the highest response has been observed for Li@$C_6O_6Li_6$ at 532 nm, followed by a similar high response for Li@$C_6O_6Li_6$ at a higher wavelength (1064 nm). Thus, we can predict that any variation in wavelength affects the response of a complex.

2.3. TD-DFT Calculations. NLO materials having high first hyperpolarizability are used in SHG for doubling of the frequency.[67,81] Thus, these NLO materials (those that have high first hyperpolarizability) must have sufficient transparency in the laser beam UV region. For this purpose, UV−vis absorption analysis of the pure $C_6O_6Li_6$ surface and doped organometallics was performed. Absorption spectroscopy calculations performed using the TD-DFT method also provides information about the absorption maxima (wavelength) of these NLO materials. None of these organometallics has shown absorption in the UV region and some part of the

https://doi.org/10.1021/acsomega.1c04349
ACS Omega 2021, 6, 29852−29861

visible region (below 500 nm). Only the pure $C_6O_6Li_6$ surface (λ_{max} = 519 nm) shows absorption in these regions, as shown in Figure 3. After doping of the pure surface, the resultant-

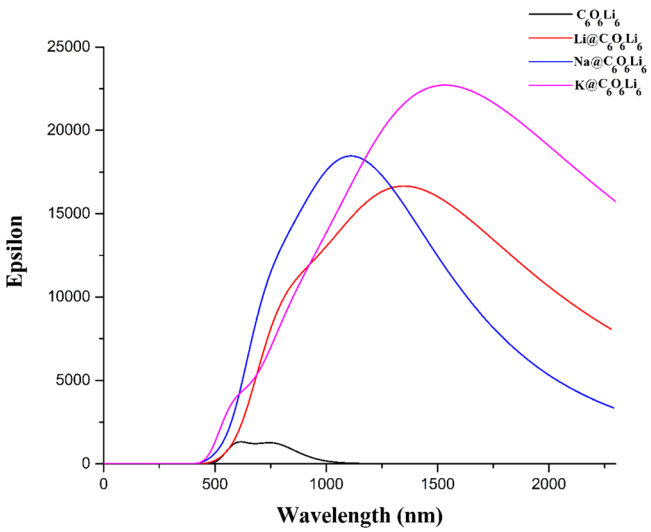

Figure 3. UV−vis spectra of pure and metal-doped $M@C_6O_6Li_6$ (M = Li, Na, and K) organometallics.

doped organometallics show a red shift to a large extent. The highest λ_{max} value (1658 nm) is obtained for $K@C_6O_6Li_6$, followed by $Li@C_6O_6Li_6$ (λ_{max} = 1438 nm), and the lowest λ_{max} value (1188 nm) is observed for $Na@C_6O_6Li_6$. A monotonic increase of the absorption maxima (wavelength) occurs with increasing atomic number of alkali metals in the dopant except for Na-doped organometallics. As the atomic size of K increases, more easily it can lose an electron to the surrounding species because the ionization potential is decreased. The Li atom has a small atomic size, so it can also shift the electronic density toward the surface. The obtained UV−vis results justify that the electronic excitation takes place in these organometallics. The HOMO−LUMO gaps are inversely proportional to the λ_{max} values, which also clarified these results. The UV−vis spectra clearly illustrate the transparency of doped organometallics, which ought to be practically used for routine laser works. The proposed organometallics can be used as efficient NLO materials in the deep-UV region because of their full transparency in the deep-UV region (≤200 nm).

3. CONCLUSIONS

In this study, we investigated the geometric, electronic, and optical properties and the NLO response of pure $C_6O_6Li_6$ and alkali metal-doped $C_6O_6Li_6$ organometallics. Thermal stabilities of the pure and doped organometallics are analyzed using interaction energy (E_{int}) calculations. Their electronic and FMO properties are also studied. The results illustrate that doping of a system with alkali metals increases the electronic density and enhances the electride character in the system via generating an excess electron system (electrons@complexant, $e^-@M@C_6O_6Li_6$, M = Li, Na, and K). The electronic density shifting is also supported by NBO charge analysis. These electrides are then investigated further for high NLO responses. The results revealed that the potassium-doped $C_6O_6Li_6$ ($K@C_6O_6Li_6$) complex has high values of first hyperpolarizability (β_o = 2.9 × 10^5 au) and a third-order NLO response (γ_{tot} 1.6 × 10^8 au), along with a high refractive index at 1064 nm, implying that the NLO response will be increased by increasing the wavelength. From these results, it is believed that these newly designed organometallics can be used in optical and optoelectronic fields for achieving better SHGs based on their electride properties.

4. COMPUTATIONAL METHODOLOGY

All calculations are performed using Gaussian 09,[82] and the results are visualized by using GaussView 5.0.[83] The geometries of pristine $C_6O_6Li_6$ and alkali metal (Li, Na, and K)-doped $C_6O_6Li_6$ complexes are optimized at the ωB97XD/6-31+G(d,p) level of theory.[84−86] Frequency calculations are also performed to confirm that the optimized structures correspond to true minima on the potential energy surface (absence of imaginary frequency). Interaction energies for the alkali metal-doped $C_6O_6Li_6$ organometallic complexes are calculated as follows

$$E_{int} = E_{C_6O_6Li_6\text{-alkali metal}} - (E_{C_6O_6Li_6} + E_{metal}) \quad (2)$$

All other parameters, that is, electronic energy, interaction energy, vertical ionization energy, NBO charges, and HOMO−LUMO gaps have been calculated using the same ωB97XD functional with the 6-31+G(d,p) basis set.

The vertical ionization energy is calculated by using the formula

$$\text{VIE} = E(X^+) - E(X) \quad (3)$$

where $E(X)$ is the energy of the neutral complex and $E(X^+)$ is the energy of the respective cation.

Parameters used for investigation of the linear optical response and nonlinear optical response include the polarizability (α_o), first hyperpolarizability (β_o), and second hyperpolarizability (γ). These parameters are calculated by using the LC-BLYP/6-311++G (2d,2p) and ωB97XD/6-311++G (2d,2p) levels of theory. LC-BLYP and ωb97XD are long-range-corrected functionals and have the correct 1.00 fraction of nonlocal exchange. They give more accurate results for noncovalent interactions[30,87,88] and optical and nonlinear optical properties.[71] The literature reveals several studies, which illustrate the reliability and validity of these functionals for the calculation of polarizability and hyperpolarizabilities.[89−93] Pople's 6-311++G (2d,2p) basis set is a suitable basis set with these functionals for the calculations of nonlinear optical properties and used in a number of recent works on nonlinear optical materials.[94] Therefore, it is also selected in this study. The static polarizability (α_o), static first hyperpolarizability (β_o), and static second hyperpolarizability (γ_{tot}) are calculated through eqs 4, 5, and 7, respectively. Furthermore, frequency-dependent NLO responses are also calculated at wavelengths 532 and 1064 nm to obtain the results, which are predominantly required by the experimentalists. These frequency-dependent NLO responses are calculated in terms of the EOPE $\beta(-\omega,\omega,0)$, electro-optical Kerr effect (EOKO) $\gamma(-\omega;\omega,0,0)$, and SHG, that is, $\beta(-2\omega,\omega,\omega)$ and $\gamma(-2\omega,\omega,\omega,0)$.

$$\alpha_o = 1/3(\alpha_{xx} + \alpha_{yy} + \alpha_{zz}) \quad (4)$$

$$\beta_o = [\beta_x^2 + \beta_y^2 + \beta_z^2]^{1/2} \quad (5)$$

Whereas eq 4 is derived as

https://doi.org/10.1021/acsomega.1c04349
ACS Omega 2021, 6, 29852−29861

$$\beta_x = \beta_{xxx} + \beta_{xyy} + \beta_{xzz}$$

$$\beta_y = \beta_{yyy} + \beta_{yzz} + \beta_{yxx} \& \beta_z = \beta_{zzz} + \beta_{zxx} + \beta_{zyy}$$

The frequency-dependent first-order hyperpolarizability is estimated as follows

$$\beta(\omega) = [\beta_x^2 + \beta_y^2 + \beta_z^2]^{1/2} \quad (6)$$

Static second hyperpolarizability (γ) can be calculated from the following equation

$$\gamma_{tot} = [\gamma_x^2 + \gamma_y^2 + \gamma_z^2]^{1/2} \quad (7)$$

The frequency-dependent second-order hyperpolarizability is estimated as follows

$$\gamma_{tot}(\omega) = [\gamma_x^2(\omega) + \gamma_y^2(\omega) + \gamma_z^2(\omega)]^{1/2} \quad (8)$$

where $\gamma_i = \left(\frac{1}{15}\right)\sum_j (\gamma_{ijji} + \gamma_{ijij} + \gamma_{iijj})i, \qquad j = \{x, y, z\}$

β_{vec} is the projection of first hyperpolarizability on the dipole moment vector, which is as follows

$$\beta_{vec} = \sum_i \frac{\mu_i \beta_i}{|\mu|} \quad (9)$$

Here, μ_i is the representation of the dipole moment in the direction of i, while $|\mu|$ is the total dipole moment of complexes, where $\beta_i = \beta_{iii}(-2\omega,\omega,\omega) + \beta_{ijj}(-2\omega,\omega,\omega) + \beta_{ikk}(-2\omega,\omega,\omega)$ for SHG and $\beta_i = \beta_{iii}(-\omega,\omega,0) + \beta_{ijj}(-\omega,\omega,0) + \beta_{ikk}(-\omega,\omega,0)$ for EOPE.

HRS is calculated as follows

$$\beta_{HRS}(-2\omega, \omega, \omega) = [\langle\beta_{zzz}^2\rangle + \langle\beta_{xzz}^2\rangle]^{1/2} \quad (10)$$

The two-level model is also applied to investigate the factors that affect the hyperpolarizability.

AUTHOR INFORMATION

Corresponding Author

Tariq Mahmood − *Department of Chemistry, COMSATS University Islamabad, Abbottabad 22060, Pakistan;* orcid.org/0000-0001-8850-9992; Phone: +92-343-7628474; Email: mahmood@cuiatd.edu.pk

Authors

Sunaina Wajid − *Department of Chemistry, COMSATS University Islamabad, Abbottabad 22060, Pakistan*

Naveen Kosar − *Department of Chemistry, University of Management and Technology (UMT), Lahore 54770, Pakistan*

Faizan Ullah − *Department of Chemistry, COMSATS University Islamabad, Abbottabad 22060, Pakistan*

Mazhar Amjad Gilani − *Department of Chemistry, COMSATS University Islamabad, Lahore 54000, Pakistan*

Khurshid Ayub − *Department of Chemistry, COMSATS University Islamabad, Abbottabad 22060, Pakistan;* orcid.org/0000-0003-0990-1860

Shabbir Muhammad − *Department of Physics, College of Science, King Khalid University, Abha 61413, Saudi Arabia*

Complete contact information is available at: https://pubs.acs.org/10.1021/acsomega.1c04349

Author Contributions

⊥S.W. and N.K. have equal contribution for the first authorship

Notes

The authors declare no competing financial interest.

ACKNOWLEDGMENTS

The author from the King Khalid University of Saudi Arabia extends his appreciation to the Deanship of Scientific Research in King Khalid University for supporting the work through project RGP.1/168/42. This study was also financially supported by the Higher Education Commission of Pakistan under a HEC indigenous fellowship to F.U. (315-19560-2PS3-146) and NRPU projects 3013 and 5309.

REFERENCES

(1) Cruzeiro, E. Z.; Tiranov, A.; Lavoie, J.; Ferrier, A.; Goldner, P.; Gisin, N.; Afzelius, M. Efficient Optical Pumping Using Hyperfine Levels in 145 Nd^{3+} :Y_2SiO_5 and Its Application to Optical Storage. *New J. Phys.* **2018**, *20*, 053013.

(2) Mande, P.; Mathew, E.; Chitrambalam, S.; Joe, I. H.; Sekar, N. NLO Properties of 1, 4-Naphthoquinone, Juglone and Lawsone by DFT and Z-Scan Technique − A Detailed Study. *Opt. Mater.* **2017**, *72*, 549−558.

(3) Demkov, A. A.; Bajaj, C.; Ekerdt, J. G.; Palmstrøm, C. J.; Ben Yoo, S. J. Materials for Emergent Silicon-Integrated Optical Computing. *J. Appl. Phys.* **2021**, *130*, 070907.

(4) Karothu, D. P.; Dushaq, G.; Ahmed, E.; Catalano, L.; Polavaram, S.; Ferreira, R.; Li, L.; Mohamed, S.; Rasras, M.; Naumov, P. Mechanically Robust Amino Acid Crystals as Fiber-Optic Transducers and Wide Bandpass Filters for Optical Communication in the near-Infrared. *Nat. Commun.* **2021**, *12*, 1326.

(5) Wada, O. Femtosecond All-Optical Devices for Ultrafast Communication and Signal Processing. *New J. Phys.* **2004**, *6*, 183.

(6) Hu, X.; Jiang, P.; Ding, C.; Yang, H.; Gong, Q. Picosecond and Low-Power All-Optical Switching Based on an Organic Photonic-Bandgap Microcavity. *Nat. Photonics* **2008**, *2*, 185−189.

(7) Hu, Y.; Tong, M.; Cheng, X. a.; Zhang, J.; Hao, H.; You, J.; Zheng, X.; Jiang, T. Bi_2Se_3 -Functionalized Metasurfaces for Ultrafast All-Optical Switching and Efficient Modulation of Terahertz Waves. *ACS Photonics* **2021**, *8*, 771−780.

(8) Janjua, M. R. S. A. Structure−Property Relationship and Systematic Study of a Series of Terpyridine Based Nonlinear Optical Compounds: DFT Computation of Interactive Design. *J. Cluster Sci.* **2019**, *30*, 45−51.

(9) Singh, L.; Zhu, G.; Mohan Kumar, G.; Revathi, D.; Pareek, P. Numerical Simulation of All-Optical Logic Functions at Micrometer Scale by Using Plasmonic Metal-Insulator-Metal (MIM) Waveguides. *Opt. Laser Technol.* **2021**, *135*, 106697.

(10) Sathiya, S.; Senthilkumar, M.; Ramachandra Raja, C. Crystal Growth, Hirshfeld Surface Analysis, DFT Study and Third Order NLO Studies of Thiourea 4 Dimethyl Aminobenzaldehyde. *J. Mol. Struct.* **2019**, *1180*, 81−88.

(11) Wang, N.; Zhang, Y.; Zhang, L. Dynamic Selection Network for Image Inpainting. *IEEE Trans. Image Process.* **2021**, *30*, 1784.

(12) Sreedharan, R.; Ravi, S.; Raghi, K. R.; Kumar, T. K. M.; Naseema, K. Growth, Linear- Nonlinear Optical Studies and Quantum Chemistry Formalism on an Organic NLO Crystal for Opto-Electronic Applications: Experimental and Theoretical Approach. *SN Appl. Sci.* **2020**, *2*, 578.

(13) Dong, J.-X.; Zhang, H.-L. Azulene-Based Organic Functional Molecules for Optoelectronics. *Chin. Chem. Lett.* **2016**, *27*, 1097−1104.

(14) Islam, N.; Pandith, A. H. Optoelectronic and Nonlinear Optical Properties of Triarylamine Helicenes: A DFT Study. *J. Mol. Model.* **2014**, *20*, 2535.

(15) Hazim, A.; Abduljalil, H. M.; Hashim, A. First Principles Calculations of Electronic, Structural and Optical Properties of (PMMA−ZrO_2−Au) and (PMMA−Al_2O_3−Au) Nanocomposites for Optoelectronics Applications. *Trans. Electr. Electron. Mater.* **2021**, *22*, 185−203.

(16) Lay-Ekuakille, A.; Massaro, A.; Singh, S. P.; Jablonski, I.; Rahman, M. Z. U.; Spano, F. Optoelectronic and Nanosensors Detection Systems: A Review. *IEEE Sens. J.* **2021**, *21*, 12645−12653.
(17) Ghosh, D.; Sarkar, K.; Devi, P.; Kim, K.-H.; Kumar, P. Current and Future Perspectives of Carbon and Graphene Quantum Dots: From Synthesis to Strategy for Building Optoelectronic and Energy Devices. *Renewable Sustainable Energy Rev.* **2021**, *135*, 110391.
(18) Dale, S. G.; Johnson, E. R. Theoretical Descriptors of Electrides. *J. Phys. Chem. A* **2018**, *122*, 9371−9391.
(19) Hosono, H.; Kitano, M. Advances in Materials and Applications of Inorganic Electrides. *Chem. Rev.* **2021**, *121*, 3121−3185.
(20) Nie, S.; Bernevig, B. A.; Wang, Z. Sixfold Excitations in Electrides. *Phys. Rev. Res.* **2021**, *3*, L012028.
(21) Yang, X.; Parrish, K.; Li, Y.-L.; Sa, B.; Zhan, H.; Zhu, Q. Switchable Two-Dimensional Electrides: A First-Principles Study. *Phys. Rev. B* **2021**, *103*, 125103.
(22) Garcia-Borràs, M.; Solà, M.; Luis, J. M.; Kirtman, B. Electronic and Vibrational Nonlinear Optical Properties of Five Representative Electrides. *J. Chem. Theory Comput.* **2012**, *8*, 2688−2697.
(23) Ahsan, A.; Khan, S.; Gilani, M. A.; Ayub, K. Endohedral Metallofullerene Electrides of $Ca_{12}O_{12}$ with Remarkable Nonlinear Optical Response. *RSC Adv.* **2021**, *11*, 1569−1580.
(24) Zhang, X.; Yang, G. Recent Advances and Applications of Inorganic Electrides. *J. Phys. Chem. Lett.* **2020**, *11*, 3841−3852.
(25) Bai, X.; Zha, X.-H.; Qiao, Y.; Qiu, N.; Zhang, Y.; Luo, K.; He, J.; Li, Q.; Huang, Q.; Francisco, J. S.; Lin, C.-T.; Du, S. Two-Dimensional Semiconducting Lu_2CT_2 (T = F, OH) MXene with Low Work Function and High Carrier Mobility. *Nanoscale* **2020**, *12*, 3795−3802.
(26) Cao, Y.-D.; Sun, Y.-H.; Shi, S.-F.; Wang, R.-M. Anisotropy of Two-Dimensional ReS_2 and Advances in Its Device Application. *Rare Met.* **2021**, *40*, 3357−3374.
(27) Weber, S.; Schäfer, S.; Saccoccio, M.; Seidel, K.; Kohlmann, H.; Gläser, R.; Schunk, S. A. Mayenite-Based Electride $C_{12}A7e^-$: An Innovative Synthetic Method via Plasma Arc Melting. *Mater. Chem. Front.* **2021**, *5*, 1301−1314.
(28) Nie, S.; Qian, Y.; Gao, J.; Fang, Z.; Weng, H.; Wang, Z. Application of Topological Quantum Chemistry in Electrides. *Phys. Rev. B* **2021**, *103*, 205133.
(29) Ellaboudy, A.; Dye, J. L.; Smith, P. B. Cesium 18-Crown-6 Compounds. A Crystalline Ceside and a Crystalline Electride. *J. Am. Chem. Soc.* **1983**, *105*, 6490−6491.
(30) Khaliq, F.; Mahmood, T.; Ayub, K.; Tabassum, S.; Gilani, M. A. Exploring Li_4N and Li_4O Superalkalis as Efficient Dopants for the $Al_{12}N_{12}$ Nanocage to Design High Performance Nonlinear Optical Materials with High Thermodynamic Stability. *Polyhedron* **2021**, *200*, 115145.
(31) Hu, Q.; Tan, R.; Li, J.; Song, W. Highly Conductive $C_{12}A7:E^-$ Electride Nanoparticles as an Electron Donor Type Promoter to P25 for Enhancing Photocatalytic Hydrogen Evolution. *J. Phys. Chem. Solids* **2021**, *149*, 109810.
(32) Das, P.; Chattaraj, P. K. Comparison Between Electride Characteristics of $Li_3@B_{40}$ and Li3@C60. *Front. Chem.* **2021**, *9*. DOI: DOI: 10.3389/fchem.2021.638581.
(33) Xiao, Y.; Zhang, X.; Li, R. $[Ca_{24}Al_{28}O_{64}]^{4+}(4e^-)$ Are Directly and Quickly Synthesized by Self-reduction of $C_{12}H_{10}Ca_3O_{14}$ + Al_2O_3 without Any Reducing Agent. *J. Am. Ceram. Soc.* **2021**, *104*, 1641−1648.
(34) Dale, S. G.; Otero-de-la-Roza, A.; Johnson, E. R. Density-Functional Description of Electrides. *Phys. Chem. Chem. Phys.* **2014**, *16*, 14584−14593.
(35) Kim, T. J.; Yoon, H.; Han, M. J. Calculating Magnetic Interactions in Organic Electrides. *Phys. Rev. B* **2018**, *97*, 214431.
(36) Saha, R.; Das, P.; Chattaraj, P. K. A Complex Containing Four Magnesium Atoms and Two Mg-Mg Bonds Behaving as an Electride. *Eur. J. Inorg. Chem.* **2019**, 4105−4111.
(37) Dale, S. G.; Johnson, E. R. The Explicit Examination of the Magnetic States of Electrides. *Phys. Chem. Chem. Phys.* **2016**, *18*, 27326−27335.
(38) Khan, K.; Tareen, A. k.; Khan, U.; Nairan, A.; Elshahat, S.; Muhammad, N.; Saeed, M.; Yadav, A.; Bibbò, L.; Ouyang, Z. Single Step Synthesis of Highly Conductive Room-Temperature Stable Cation-Substituted Mayenite Electride Target and Thin Film. *Sci. Rep.* **2019**, *9*, 4967.
(39) Lee, S. Y.; Hwang, J.-Y.; Park, J.; Nandadasa, C. N.; Kim, Y.; Bang, J.; Lee, K.; Lee, K. H.; Zhang, Y.; Ma, Y.; Hosono, H.; Lee, Y. H.; Kim, S.-G.; Kim, S. W. Ferromagnetic Quasi-Atomic Electrons in Two-Dimensional Electride. *Nat. Commun.* **2020**, *11*, 1526.
(40) Matsuishi, S.; Toda, Y.; Miyakawa, M.; Hayashi, K.; Kamiya, T.; Hirano, M.; Tanaka, I.; Hosono, H. High-Density Electron Anions in a Nanoporous Single Crystal: $[Ca_{24}Al_{28}O_{64}]^{4+}(4e^-)$. *Science* **2003**, *301*, 626−629.
(41) Hayashi, F.; Tomota, Y.; Kitano, M.; Toda, Y.; Yokoyama, T.; Hosono, H. NH^{2-} Dianion Entrapped in a Nanoporous $12CaO\cdot 7Al_2O_3$ Crystal by Ammonothermal Treatment: Reaction Pathways, Dynamics, and Chemical Stability. *J. Am. Chem. Soc.* **2014**, *136*, 11698−11706.
(42) Hosono, H.; Kim, J.; Toda, Y.; Kamiya, T.; Watanabe, S. Transparent Amorphous Oxide Semiconductors for Organic Electronics: Application to Inverted OLEDs. *Proc. Natl. Acad. Sci. U.S.A.* **2017**, *114*, 233−238.
(43) Zhang, Y.; Wang, H.; Wang, Y.; Zhang, L.; Ma, Y. Computer-Assisted Inverse Design of Inorganic Electrides. *Phys. Rev. X* **2017**, *7*, 011017.
(44) Kulichenko, M.; Fedik, N.; Bozhenko, K. V.; Boldyrev, A. I. Inorganic Molecular Electride Mg_4O_3 : Structure, Bonding, and Nonlinear Optical Properties. *Chem.—Eur. J.* **2019**, *25*, 5311−5315.
(45) Wang, Y.-F.; Qin, T.; Tang, J.-M.; Liu, Y.-J.; Xie, M.; Li, J.; Huang, J.; Li, Z.-R. Novel inorganic aromatic mixed-valent superalkali electride CaN3Ca: an alkaline-earth-based high-sensitivity multi-state nonlinear optical molecular switch. *Phys. Chem. Chem. Phys.* **2020**, *22*, 5985−5994.
(46) Liyanage, P. S.; de Silva, R. M.; de Silva, K. M. N. Nonlinear Optical (NLO) Properties of Novel Organometallic Complexes: High Accuracy Density Functional Theory (DFT) Calculations. *J. Mol. Struct.: THEOCHEM* **2003**, *639*, 195−201.
(47) de Silva, I. C.; de Silva, R. M.; Nalin de Silva, K. M. Investigations of Nonlinear Optical (NLO) Properties of Fe, Ru and Os Organometallic Complexes Using High Accuracy Density Functional Theory (DFT) Calculations. *J. Mol. Struct.: THEOCHEM* **2005**, *728*, 141−145.
(48) Dairi, M.; Elhorri, A. M.; Tchouar, N.; Boumedel, H.; Azizi, S. Theoretical Study by DFT of Organometallic Complexes Based on Metallocenes Active in NLO. *J. Mol. Model.* **2021**, *27*, 179.
(49) Taboukhat, S.; Kichou, N.; Fillaut, J.-L.; Alévêque, O.; Waszkowska, K.; Zawadzka, A.; El-Ghayoury, A.; Migalska-Zalas, A.; Sahraoui, B. Transition Metals Induce Control of Enhanced NLO Properties of Functionalized Organometallic Complexes under Laser Modulations. *Sci. Rep.* **2020**, *10*, 15292.
(50) Zhong, R.-L.; Xu, H.-L.; Li, Z.-R.; Su, Z.-M. Role of Excess Electrons in Nonlinear Optical Response. *J. Phys. Chem. Lett.* **2015**, *6*, 612−619.
(51) Irshad, S.; Ullah, F.; Khan, S.; Ludwig, R.; Mahmood, T.; Ayub, K. First Row Transition Metals Decorated Boron Phosphide Nanoclusters as Nonlinear Optical Materials with High Thermodynamic Stability and Enhanced Electronic Properties; A Detailed Quantum Chemical Study. *Opt. Laser Technol.* **2021**, *134*, 106570.
(52) Mallah, R. R.; Mohbiya, D. R.; Sreenath, M. C.; Chitrambalam, S.; Joe, I. H.; Sekar, N. Fluorescent Meso-Benzyl Curcuminoid Boron Complex: Synthesis, Photophysics, DFT and NLO Study. *Opt. Mater.* **2018**, *84*, 786−794.
(53) Mejía-Hernández, F. G.; Hernández-Ortíz, O. J.; Muñoz-Pérez, F. M.; Martínez-Pérez, A. I.; Vázquez-García, R. A.; Vera-Cárdenas, E. E.; Ortega-Mendoza, J. G.; Veloz-Rodríguez, M. A.; Rueda-Soriano, E.; Alemán-Ayala, K. Mechanochemical Synthesis, Linear and Nonlinear Optical Properties of a New Oligophenyleneimine with Indole Terminal Moiety for Optoelectronic Application. *J. Mater. Sci.: Mater. Electron.* **2021**, *32*, 6283−6295.

(54) Ahsin, A.; Ayub, K. Oxacarbon superalkali C3X3Y3 (X = O, S and Y = Li, Na, K) clusters as excess electron compounds for remarkable static and dynamic NLO response. *J. Mol. Graphics Modell.* **2021**, *106*, 107922.
(55) Nazeer, U.; Rasool, N.; Mujahid, A.; Mansha, A.; Zubair, M.; Kosar, N.; Mahmood, T.; Raza Shah, A.; Shah, S. A. A.; Zakaria, Z. A.; Akhtar, M. N. Selective Arylation of 2-Bromo-4-Chlorophenyl-2-Bromobutanoate via a Pd-Catalyzed Suzuki Cross-Coupling Reaction and Its Electronic and Non-Linear Optical (NLO) Properties via DFT Studies. *Molecules* **2020**, *25*, 3521.
(56) Savithiri, S.; Bharanidharan, S.; Sugumar, P.; Rajeevgandhi, C.; Indhira, M. Synthesis, spectral, stereochemical, biological, molecular docking and DFT studies of 3-alkyl/3,5-dialkyl-2r,6c-di(naphthyl)-piperidin-4-one picrates derivatives. *J. Mol. Struct.* **2021**, *1234*, 130145.
(57) Liu, Y.; Merinov, B. V.; Goddard, W. A. Origin of Low Sodium Capacity in Graphite and Generally Weak Substrate Binding of Na and Mg among Alkali and Alkaline Earth Metals. *Proc. Natl. Acad. Sci. U.S.A.* **2016**, *113*, 3735−3739.
(58) Sohail, M.; Khaliq, F.; Mahmood, T.; Ayub, K.; Tabassum, S.; Gilani, M. A. Influence of Bi-Alkali Metals Doping over $Al_{12}N_{12}$ Nanocage on Stability and Optoelectronic Properties: A DFT Investigation. *Radiat. Phys. Chem.* **2021**, *184*, 109457.
(59) Hou, N.; Wu, Y.; Wu, H. The Influence of Alkali Metals Interaction with Al/P-Substituted BN Nanosheets on Their Electronic and Nonlinear Optical Properties: A DFT Theoretical Study. *ChemistrySelect* **2019**, *4*, 1441−1447.
(60) Ayub, K. Are Phosphide Nano-Cages Better than Nitride Nano-Cages? A Kinetic, Thermodynamic and Non-Linear Optical Properties Study of Alkali Metal Encapsulated X 12 Y 12 Nano-Cages. *J. Mater. Chem. C* **2016**, *4*, 10919−10934.
(61) Shehzad, R. A.; Iqbal, J.; Ayub, K.; Nawaz, F.; Muhammad, S.; Ayub, A. R.; Iqbal, S. Enhanced Linear and Nonlinear Optical Response of Superhalogen (Al7) Doped Graphitic Carbon Nitride (g-C3N4). *Optik* **2021**, *226*, 165923.
(62) Xu, H.-L.; Wang, F.-F.; Chen, W.; Yu, G.-T. The Complexant Shape Effect on First (Hyper)Polarizability of Alkalides $Li^+(NH_2CH_3)_4$ M − (M = Li, Na, and K). *Int. J. Quantum Chem.* **2011**, *111*, 3174−3183.
(63) Song, Y.-D.; Wang, L.; Wu, L.-M. How the Alkali Metal Atoms Affect Electronic Structure and the Nonlinear Optical Properties of $C_{24}N_{24}$ Nanocage. *Optik* **2017**, *135*, 139−152.
(64) Teng, Y.; Sheng, Q.; Weng, H.; Zhou, Z.; Huang, X.; Li, Z.; Zhang, T. Theoretical Study of a Novel Organic Electride with Large Nonlinear Optical Responses. *Int. J. Quantum Chem.* **2020**, *120*, No. e26235.
(65) Ullah, F.; Ayub, K.; Mahmood, T. Remarkable Second and Third Order Nonlinear Optical Properties of Organometallic C_6Li_6 $-M_3O$ Electrides. *New J. Chem.* **2020**, *44*, 9822−9829.
(66) Kosar, N.; Tahir, H.; Ayub, K.; Mahmood, T. DFT Studies of Single and Multiple Alkali Metals Doped C_{24} Fullerene for Electronics and Nonlinear Optical Applications. *J. Mol. Graphics Modell.* **2021**, *105*, 107867.
(67) Kosar, N.; Mahmood, T.; Ayub, K.; Tabassum, S.; Arshad, M.; Gilani, M. A. Doping Superalkali on $Zn_{12}O_{12}$ Nanocage Constitutes a Superior Approach to Fabricate Stable and High-Performance Nonlinear Optical Materials. *Opt. Laser Technol.* **2019**, *120*, 105753.
(68) Chandiramouli, R.; Srivastava, A.; Nagarajan, V. NO Adsorption Studies on Silicene Nanosheet: DFT Investigation. *Appl. Surf. Sci.* **2015**, *351*, 662−672.
(69) Morisawa, Y.; Tachibana, S.; Ikehata, A.; Yang, T.; Ehara, M.; Ozaki, Y. Changes in the Electronic States of Low-Temperature Solid n-Tetradecane: Decrease in the HOMO-LUMO Gap. *ACS Omega* **2017**, *2*, 618−625.
(70) He, H.-M.; Luis, J. M.; Chen, W.-H.; Yu, D.; Li, Y.; Wu, D.; Sun, W.-M.; Li, Z.-R. Nonlinear Optical Response of Endohedral All-Metal Electride Cages $2e^-$ Mg^{2+} $(M@E_{12})^{2-}Ca^{2+}$ (M = Ni, Pd, and Pt; E = Ge, Sn, and Pb). *J. Mater. Chem. C* **2019**, *7*, 645−653.
(71) Ullah, F.; Kosar, N.; Ayub, K.; Mahmood, T. Superalkalis as a Source of Diffuse Excess Electrons in Newly Designed Inorganic Electrides with Remarkable Nonlinear Response and Deep Ultraviolet Transparency: A DFT Study. *Appl. Surf. Sci.* **2019**, *483*, 1118−1128.
(72) Bae, S.; Espinosa-García, W.; Kang, Y. G.; Egawa, N.; Lee, J.; Kuwahata, K.; Khazaei, M.; Ohno, K.; Kim, Y. H.; Han, M. J.; Hosono, H.; Dalpian, G. M.; Raebiger, H. MXene Phase with C 3 Structure Unit: A Family of 2D Electrides. *Adv. Funct. Mater.* **2021**, *31*, 2100009.
(73) Tahmasebi, E.; Shakerzadeh, E.; Biglari, Z. Theoretical Assessment of the Electro-Optical Features of the Group III Nitrides ($B_{12}N_{12}$, $Al_{12}N_{12}$ and $Ga_{12}N_{12}$) and Group IV Carbides (C_{24}, $Si_{12}C_{12}$ and $Ge_{12}C_{12}$) Nanoclusters Encapsulated with Alkali Metals (Li, Na and K). *Appl. Surf. Sci.* **2016**, *363*, 197−208.
(74) Buldakov, M. A.; Koryukina, E. V.; Cherepanov, V. N.; Kalugina, Y. N. A Dipole-Moment Function of MeH Molecules (Me = Li, Na, K)). *Russ. Phys. J.* **2007**, *50*, 532−537.
(75) Li, X.; Zhang, Y.; Lu, J. Remarkably Enhanced First Hyperpolarizability and Nonlinear Refractive Index of Novel Graphdiyne-Based Materials for Promising Optoelectronic Applications: A First-Principles Study. *Appl. Surf. Sci.* **2020**, *512*, 145544.
(76) Mondal, A.; Hatua, K.; Nandi, P. K. Why Lithiation Results Large Enhancement of Second Hyperpolarizability of Delta Shaped Complexes M-C_2H_2 (M = Be, Mg and Ca)? *Chem. Phys. Lett.* **2019**, *720*, 36−41.
(77) Li, Z.-J.; Wang, F.-F.; Li, Z.-R.; Xu, H.-L.; Huang, X.-R.; Wu, D.; Chen, W.; Yu, G.-T.; Gu, F. L.; Aoki, Y. Large Static First and Second Hyperpolarizabilities Dominated by Excess Electron Transition for Radical Ion Pair Salts M $_2$* + TCNQ*− (M = Li, Na, K). *Phys. Chem. Chem. Phys.* **2009**, *11*, 402−408.
(78) Lu, T.; Chen, F. Multiwfn: A multifunctional wavefunction analyzer. *J. Comput. Chem.* **2012**, *33*, 580−592.
(79) Souza, T. E.; Rosa, I. M. L.; Legendre, A. O.; Paschoal, D.; Maia, L. J. Q.; Dos Santos, H. F.; Martins, F. T.; Doriguetto, A. C. Non-centrosymmetric crystals of newN-benzylideneaniline derivatives as potential materials for non-linear optics. *Acta Crystallogr., Sect. B: Struct. Sci., Cryst. Eng. Mater.* **2015**, *71*, 416−426.
(80) Campo, J.; Wenseleers, W.; Goovaerts, E.; Szablewski, M.; Cross, G. H. Accurate Determination and Modeling of the Dispersion of the First Hyperpolarizability of an Efficient Zwitterionic Nonlinear Optical Chromophore by Tunable Wavelength Hyper-Rayleigh Scattering. *J. Phys. Chem. C* **2008**, *112*, 287−296.
(81) Arun Kumar, R.; Arivanandhan, M.; Hayakawa, Y. Recent Advances in Rare Earth-Based Borate Single Crystals: Potential Materials for Nonlinear Optical and Laser Applications. *Prog. Cryst. Growth Charact. Mater.* **2013**, *59*, 113−132.
(82) Frisch, M. J.; Trucks, G. W.; Schlegel, H. B.; Scuseria, G. E.; Robb, M. A.; Cheeseman, J. R.; Scalmani, G.; Barone, V.; Mennucci, B.; Petersson, G. A.; Nakatsuji, H.; Caricato, M.; Li, X.; Hratchian, H. P.; Izmaylov, A. F.; Bloino, J.; Zheng, G.; Sonnenberg; Hada, M.; Ehara, M.; Toyota, K.; Fukuda, R.; Hasegawa, J.; Ishida, M.; Nakajima, T.; Honda, Y.; Kitao, O.; Nakai, H.; Vreven, T.; Montgomery, J. A.; Peralta, J. E.; Ogliaro, F.; Bearpark, M.; Heyd, J. J.; Brothers, E.; Kudin, K. N.; Staroverov, V. N.; Normand, R. K. J.; Raghavachari, K.; Rendell, A.; Burant, J. C.; Iyengar, S. S.; Tomasi, J.; Rega, N.; Millam, J. M.; Klene, M.; Knox, J. E.; Cross, J. B.; Bakken, V.; Adamo, C.; Gomperts, R.; Stratmann, R. E.; Yazyev, O.; Austin, A. J.; Cammi, R.; Pomelli, C.; Ochterski, J. W.; Martin, R. L.; Morokuma, K.; Zakrzewski, V. G.; Voth, G. A.; Salvador, P.; Dannenberg, J. J.; Dapprich, S.; Daniels, A. D.; Farkas, Ö.; Foresman, J. B.; Ortiz, J. V.; Cioslowski, J. *Gaussian 09*, Revision D.01; Gaussian, Inc: Wallingford CT, 2009.
(83) Dennington, R.; Keith, T.; Millam, J. *GaussView*, Version 5, 2009.
(84) Sajid, H.; Khan, S.; Ayub, K.; Mahmood, T. Effective Adsorption of A-Series Chemical Warfare Agents on Graphdiyne Nanoflake: A DFT Study. *J. Mol. Model.* **2021**, *27*, 117.
(85) Kosar, N.; Ayub, K.; Mahmood, T. Surface Functionalization of Twisted Graphene $C_{32}H_{15}$ and $C_{104}H_{52}$ Derivatives with Alkalis and

Superalkalis for NLO Response; a DFT Study. *J. Mol. Graphics Modell.* **2021**, *102*, 107794.
(86) Kosar, N.; Tahir, H.; Ayub, K.; Gilani, M. A.; Mahmood, T. Theoretical Modification of C24 Fullerene with Single and Multiple Alkaline Earth Metal Atoms for Their Potential Use as NLO Materials. *J. Phys. Chem. Solids* **2021**, *152*, 109972.
(87) Sajid, H.; Ullah, F.; Khan, S.; Ayub, K.; Arshad, M.; Mahmood, T. Remarkable Static and Dynamic NLO Response of Alkali and Superalkali Doped Macrocyclic [Hexa-]Thiophene Complexes; a DFT Approach. *RSC Adv.* **2021**, *11*, 4118−4128.
(88) Khan, P.; Mahmood, T.; Ayub, K.; Tabassum, S.; Amjad Gilani, M. Turning Diamondoids into Nonlinear Optical Materials by Alkali Metal Substitution: A DFT Investigation. *Opt. Laser Technol.* **2021**, *142*, 107231.
(89) Oviedo, M. B.; Ilawe, N. V.; Wong, B. M. Polarizabilities of π-Conjugated Chains Revisited: Improved Results from Broken-Symmetry Range-Separated DFT and New CCSD(T) Benchmarks. *J. Chem. Theory Comput.* **2016**, *12*, 3593−3602.
(90) Xu, L.; Kumar, A.; Wong, B. M. Linear polarizabilities and second hyperpolarizabilities of streptocyanines: Results from broken-Symmetry DFT and new CCSD(T) benchmarks. *J. Comput. Chem.* **2018**, *39*, 2350−2359.
(91) Khan, S.; Gilani, M. A.; Munsif, S.; Muhammad, S.; Ludwig, R.; Ayub, K. Inorganic Electrides of Alkali Metal Doped $Zn_{12}O_{12}$ Nanocage with Excellent Nonlinear Optical Response. *J. Mol. Graphics Modell.* **2021**, *106*, 107935.
(92) Ahsan, A.; Ayub, K. Extremely Large Nonlinear Optical Response and Excellent Electronic Stability of True Alkaline Earthides Based on Hexaammine Complexant. *J. Mol. Liq.* **2020**, *297*, 111899.
(93) Ahsan, A.; Ayub, K. Adamanzane Based Alkaline Earthides with Excellent Nonlinear Optical Response and Ultraviolet Transparency. *Opt. Laser Technol.* **2020**, *129*, 106298.
(94) Torrent-Sucarrat, M.; Solà, M.; Duran, M.; Luis, J. M.; Kirtman, B. Basis Set and Electron Correlation Effects on Initial Convergence for Vibrational Nonlinear Optical Properties of Conjugated Organic Molecules. *J. Chem. Phys.* **2004**, *120*, 6346−6355.

https://doi.org/10.1021/acsomega.1c04349
ACS Omega 2021, 6, 29852−29861